

**Synthesis and luminescent properties of  $(RE_{0.95}Ln_{0.05})_2O_2S$  (RE = La, Y; Ln = Ho, Tm)**

Sal'nikova E.I., Denisenko Yu.G., Kolesnikov I.E., Lähderanta E., Andreev O.V., Azarapin N.O., Basova S.A., Gubin A.A., Oreshonkov A.S.

This is a Post-print version of a publication  
published by Elsevier  
in Journal of Solid State Chemistry

DOI: 10.1016/j.jssc.2020.121753

**Copyright of the original publication:** © 2020 Elsevier

**Please cite the publication as follows:**

Sal'nikova, E.I., Denisenko, Yu.G., Kolesnikov, I.E., Lähderanta, E., Andreev, O.V., Azarapin, N. O., Basova, S.A., Gubin, A.A., Oreshonkov, A.S. (2021). Synthesis and luminescent properties of  $(RE_{0.95}Ln_{0.05})_2O_2S$  (RE = La, Y; Ln = Ho, Tm). Journal of Solid State Chemistry, vol. 293. DOI: 10.1016/j.jssc.2020.121753

**This is a parallel published version of an original publication.  
This version can differ from the original published article.**

1 Corresponding author: E.I. Sal'nikova  
2 Department of Inorganic and Physical Chemistry,  
3 State University of Tyumen, Tyumen 625000, Russia  
4 Phone: +7 9324840538  
5 E-mail: elenasalnikova213@gmail.com

6  
7  
8 **SYNTHESIS AND LUMINESCENT PROPERTIES OF  $\text{RE}_2\text{O}_2\text{S}:\text{Ln}^{3+}$**   
9 **(RE = La, Y; Ln = Ho, Tm)**

10  
11 E.I. Sal'nikova<sup>1,2</sup>, Yu.G. Denisenko<sup>3</sup>, I.E. Kolesnikov<sup>4,5</sup>, E. Lähderanta<sup>5</sup>, O.V. Andreev<sup>1,6</sup>,  
12 N.O. Azarapin<sup>1</sup>, S.A. Basova<sup>1</sup>, Gubin A.A.<sup>7</sup>

13 1.

14 <sup>1</sup>Department of Inorganic and Physical Chemistry, Tyumen State University, Tyumen 625003,  
15 Russia

16 <sup>2</sup>Komissarov Department of General Chemistry, Northern Trans-Ural Agricultural University,  
17 Tyumen, 625003, Russia

18 <sup>3</sup>Department of General and Special Chemistry, Industrial University of Tyumen, Tyumen 625000,  
19 Russia

20 <sup>4</sup>Center for Optical and Laser Materials Research, St. Petersburg State University, St. Petersburg  
21 199034, Russia

22 <sup>5</sup>Department of Physics, Lappeenranta University of Technology LUT, Lappeenranta 53850,  
23 Finland

24 <sup>6</sup>Laboratory of the Chemistry of Rare Earth compounds, Institute of Solid State Chemistry, UB  
25 RAS, 620137 Ekaterinburg, Russia

26 <sup>7</sup>Laboratory of Electron and Probe Microscopy, Tyumen State University, Tyumen 625003, Russia  
27

28 **Abstract**

29 Solid solutions of oxysulfides  $\text{RE}_2\text{O}_2\text{S}:\text{Ln}$  (RE = La, Y) were obtained by hydrogen reduction of the  
30 co-precipitated sulfates followed by sulfidation of the reaction products. The crystal chemical  
31 characteristics of the obtained compounds were refined by the Rietveld method. Morphological  
32 certification of particles in the dynamics of synthesis was carried out. The results showed an  
33 increase in particle size and the appearance of spherical holes of 50-400 nm due to elevated  
34 temperatures and the diffusion nature of reduction and sulfidation processes. Steady state  
35 luminescence properties displayed characteristic sharp bands corresponding to 4f-4f transitions.  
36 Luminescence decay curves of all studied samples showed monoexponential decay with  
37 microsecond and hundreds microsecond lifetimes depending on doping ions. Calculated color  
38 coordinates of  $\text{Ho}^{3+}$  and  $\text{Tm}^{3+}$ -doped powders make them promising candidates to be used as  
39 phosphors.

40  
41 **Keywords:** rare earth oxysulfides, synthesis, Rietveld, luminescence, lifetime, quantum yield  
42  
43

44

## 45 **1. Introduction**

46 The rare-earth oxysulfides  $\text{La}_2\text{O}_2\text{S}$  ( $\text{La}^0 [\text{Xe}]5d^16s^2$ ),  $\text{Gd}_2\text{O}_2\text{S}$  ( $\text{Gd}^0 [\text{Xe}]4f^75d^16s^2$ ),  $\text{Y}_2\text{O}_2\text{S}$   
47 ( $\text{Y}^0 [\text{Xe}]5d^15s^2$ ),  $\text{Lu}_2\text{O}_2\text{S}$  ( $\text{Lu}^0 [\text{Xe}]4f^{14}5d^16s^2$ ), due to the peculiarities of their electronic structure,  
48 can be regarded as unique luminescent structures for practical use and for basic research [1, 2].  
49 Luminescence is mainly determined by the nature of the activator ion, but the host matrix into  
50 which this ion is embedded affects the intensity of the emission lines through its crystal field [3, 4].

51 Compounds  $\text{RE}_2\text{O}_2\text{S}:\text{Ln}^{3+}$  are in great demand due to their excellent luminescent properties  
52 and color purity [5]. They can be suitable for creating thermographic phosphors (excellent  
53 candidates for fluorescence measurements of physiological temperatures using a miniature  
54 temperature sensor up to nanoscale) [6]. The authors of [7-12] synthesized and studied the  
55 properties of new materials that demonstrate unique thermal and luminescent properties.

56 Most phosphors are excited by ultraviolet light and exhibit temperature sensitivity, which  
57 allows them to be used to control temperature conditions in gas turbine combustion chambers in  
58 high-temperature areas of the turbine [13], as well as in X-ray diffraction and scintillation  
59 equipment [14]. These materials have the ability to store and release large volumes of oxygen under  
60 oxidation/reduction conditions, which makes them interesting as nanocatalysts [15], allows them to  
61 be used as laser detection of securities counterfeits [16], to create ultraviolet LEDs (white lamps  
62 light) [17], in photovoltaic solar cells [18], as a coating of reinforcing screens during magnetic  
63 resonance imaging [19].

64 Nanophosphors are a class of materials with unique properties that make them very  
65 attractive for biological applications [20]. Information about the compositions studied in this paper  
66 is rather limited. The optical fluorescence of ten trivalent lanthanide ions, Pr, Nd, Sm, Eu, Gd, Tb,  
67 Dy, Ho, Er, and Tm in  $\text{Y}_2\text{O}_2\text{S}$ ,  $\text{La}_2\text{O}_2\text{S}$ , and  $\text{Gd}_2\text{O}_2\text{S}$ , which was measured using X-ray excitation at  
68 300 K., was described in [21].  $\text{La}_2\text{O}_2\text{S}$  appears to be a more efficient host than  $\text{Y}_2\text{O}_2\text{S}$  and  $\text{Gd}_2\text{O}_2\text{S}$   
69 for all lanthanides. The main features of the luminescence spectra and kinetics of  $(\text{Y}_{1-x}\text{Tm}_x)_2\text{O}_2\text{S}$   
70 solid solutions in the range 400–2000 nm under laser excitation at 790 and 810 nm were studied.  
71 The results were used to develop a series of IR phosphors that are “invisible” under laser excitation  
72 in the range of 790–810 nm and possess tunable and reproducible relative intensities of the three  
73 groups of IR luminescence bands in the ranges of 770–840, 1360–1520, and 1650–1980 nm,  
74 respectively [22]. The compound  $\text{La}_2\text{O}_2\text{S}:\text{Tm}^{3+}$  was studied in [23]; luminescence excitation at a  
75 wavelength above 355 nm occurs mainly due to energy transfer from the host, which absorbs the  
76 exciting radiation, to the  $\text{Tm}^{3+}$  ion.

77 The method of obtaining new functional materials  $\text{RE}_2\text{O}_2\text{S}:\text{Ln}$  by sequential processing of  
78 powders of sulfates of rare-earth elements in a stream of  $\text{H}_2$ ,  $\text{H}_2\text{S}$ , used in this work, has several

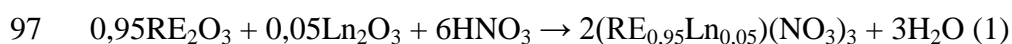
79 advantages over solid-state synthesis methods. It is distinguished by manufacturability, productivity,  
80 the ability to produce batches of the product from tens to hundreds of grams and to conduct the  
81 process both continuously and interrupted at any time, without any significant negative  
82 consequences [24].

83 Thus, the aim of the work is to obtain solid solutions of oxysulfides by sequential processing  
84 of co-precipitated sulfates of rare-earth elements in an atmosphere of H<sub>2</sub>, H<sub>2</sub>S, and to study the  
85 morphology and optical properties of the obtained samples.

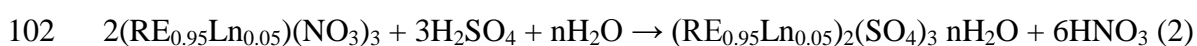
## 86 87 **2. Materials and methods**

### 88 **2a. Preparative Methods**

89 For the synthesis of RE<sub>2</sub>O<sub>2</sub>S:Ln<sup>3+</sup> compounds, calculated in a ratio of 95:5 mol. % of the  
90 amount of Ln<sub>2</sub>O<sub>3</sub> (≥99.99%, ultrapure, OOO TDM-96, Russia). Oxide powders were weighed on an  
91 analytical balance to an accuracy of ± 0.0001 g. Before weighing, the oxides were calcined in a  
92 muffle furnace at 900 °C for 24 hours to remove sorbed water, as well as rare earth carbonates and  
93 hydroxides. Acids were selected using graduated pipettes with an accuracy of ± 0.1 ml. Samples of  
94 oxides were poured into a heat-resistant glass with a capacity of 100 ml, then HNO<sub>3</sub> (Vekton Ltd.,  
95 Russia) was poured with constant stirring, with a concentration of 15 mol/L, with a volume of 10  
96 ml, if necessary, heated to a transparent state. The result was a mixture of nitrates:



98 Then, nitrate solutions were cooled to a temperature of 35-40 °C and 7 ml of H<sub>2</sub>SO<sub>4</sub> (Vekton  
99 Ltd., Russia), with a concentration of 18 mol/L, with an excess of up to 7%, were added with a fine  
100 stream with constant stirring. As a result, crystalline hydrates of the precipitated co-crystallized  
101 sulfates were obtained according to the chemical reaction equation:

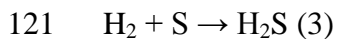


103 The resulting suspension was evaporated to dryness at 85-90 °C to remove water and  
104 nitrogen oxides, and then calcined at 600 °C for up to 12 hours to release residual sulfuric acid and  
105 achieve high crystallinity of the sample. The method of co-precipitation of sulfates allows to  
106 achieve a uniform distribution of rare-earth metal cations. The resulting precipitate was triturated to  
107 obtain a powder and sieved through a sieve with a 100 μm cell.

108 The sample was treated in a hydrogen stream using the setup shown in Figure S1. Hydrogen  
109 synthesis was performed using a SPECTR-6M hydrogen generator. Bidistilled water passed through  
110 a deionizer was used for electrolysis of water. A 10 g sulphate powder was placed in a quartz glass  
111 located in a reactor with a gas outlet tube placed in it. The device was carefully sealed and purged in  
112 a stream of hydrogen for 30 minutes in order to displace air from it with a gas flow rate of 7-8 l/h  
113 from the hydrogen generator, and then placed in a vertical furnace, setting the temperature mode  
114 using the Thermolux controller. After processing the sample for 1 hour at 620 °C in a stream of H<sub>2</sub>,

115 the reactor was taken out of the furnace, cooled, and a sample was taken to study the phase  
116 composition. To complete the passage of chemical transformations, the treatment in a stream of  
117 hydrogen was carried out for up to 4 hours.

118 Processing in the H<sub>2</sub>S stream was carried out in a similar way, only for the synthesis of  
119 hydrogen sulfide, an additional furnace was used, in which a reactor with sulfur (molten) melted at  
120 400 °C was placed (Figure S2). The formation of hydrogen sulfide occurred by the reaction:



122

## 123 **2b. Physico-chemical Analysis Methods**

124 X-ray phase analysis (XRD) was carried out on a BRUKER D2 PHASER diffractometer  
125 with a linear detector LYNXEYE (CuK $\alpha$  radiation, Ni filter). Rietveld refinement of all samples  
126 was performed using TOPAS 4.2 [25]. All fixed reflexes of the obtained phases were indexed.

127 Micrographs of powder particles from the processing steps in a stream of H<sub>2</sub>, H<sub>2</sub>S were  
128 obtained using a JEOL JSM-6510LV scanning electron microscope.

129 All photoluminescence measurements were carried out on a research grade  
130 spectrofluorometer Fluorolog-3 (Horiba Jobin Yvon) equipped with dual monochromators for  
131 excitation and emission channels and a 450 W xenon lamp as an excitation source. Lifetime  
132 measurements were performed at the same device using Xe-flash lamp (150 W power, 3  $\mu$ s pulse  
133 width). The integration sphere (Quanta- $\phi$ , 6 inches) was used to measure the quantum yield. The  
134 measurements were carried out with powders according to the guide provided by manufacturer  
135 (four spectra-based measurement).

136

## 137 **3. Results and discussions**

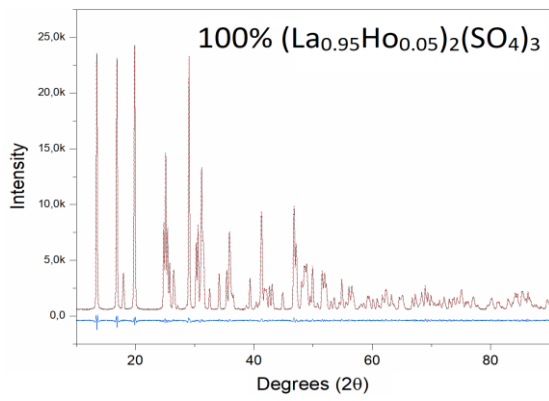
138

139 Two compositions were chosen as a model for discussing the results of sample synthesis:

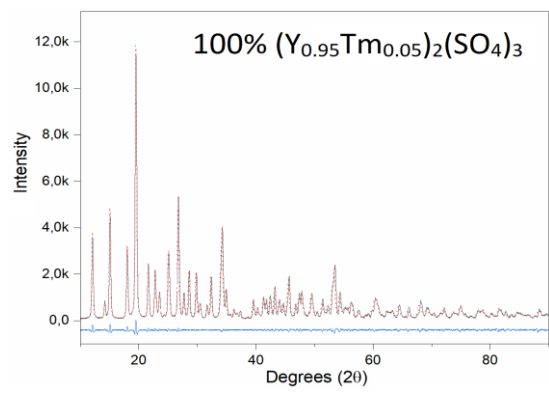
140 La<sub>2</sub>(SO<sub>4</sub>)<sub>3</sub>: Ho<sup>3+</sup> (5 mol %) and Y<sub>2</sub>(SO<sub>4</sub>)<sub>3</sub>: Tm<sup>3+</sup> (5 mol %). Figure 1 presents a complete picture of  
141 the chemical transformations that occur during the heat treatment of sulfates in a stream of H<sub>2</sub>, H<sub>2</sub>S.  
142 The remaining samples were synthesized by the same procedure.

143 The starting materials for the synthesis of solid solutions of oxysulfides are sulfates (Figure  
144 1, a, b), in which the doping ion is embedded in the host crystal. According to x-ray phase analysis,  
145 they are single-phase, which proves the formation of solid solutions of rare-earth sulfates.

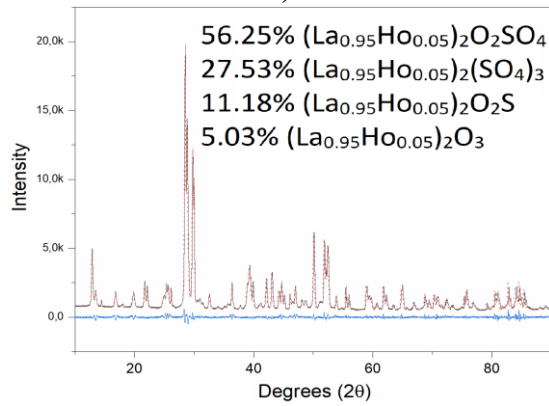
146 For greater reliability, we trace the detailed formation of phases using the example of a  
147 sample of lanthanum-holmium sulfate. The appearance of gaseous reaction products at 610 °C  
148 allows processing in a stream of hydrogen at 620 °C for 1 hour in order to draw up the equations of  
149 chemical reactions based on the results of X-ray phase analysis. As a result of processing, 4 phases  
150 were found in the powder composition: (La<sub>0.95</sub>Ho<sub>0.05</sub>)<sub>2</sub>(SO<sub>4</sub>)<sub>3</sub> - (La<sub>0.95</sub>Ho<sub>0.05</sub>)<sub>2</sub>O<sub>2</sub>SO<sub>4</sub> -  
151 (La<sub>0.95</sub>Ho<sub>0.05</sub>)<sub>2</sub>O<sub>2</sub>S - La<sub>0.95</sub>Ho<sub>0.05</sub>)<sub>2</sub>O<sub>3</sub> (Fig. 1, c).



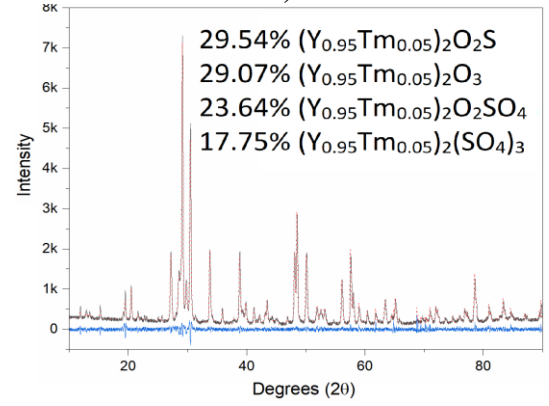
**a)**



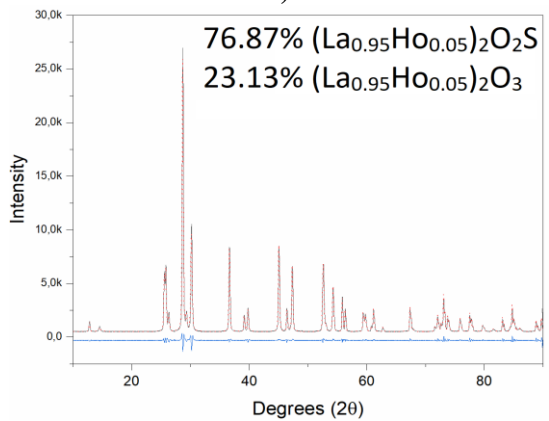
**b)**



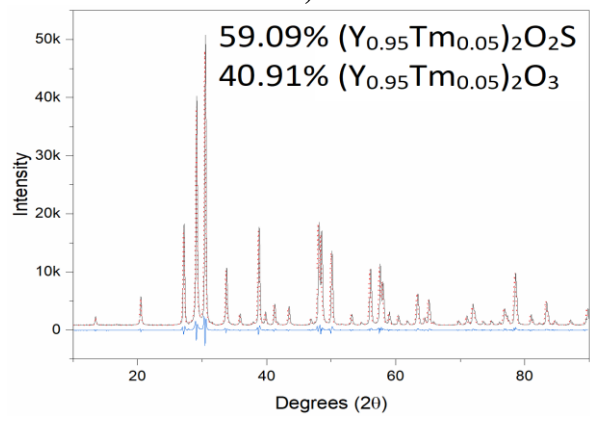
**c)**



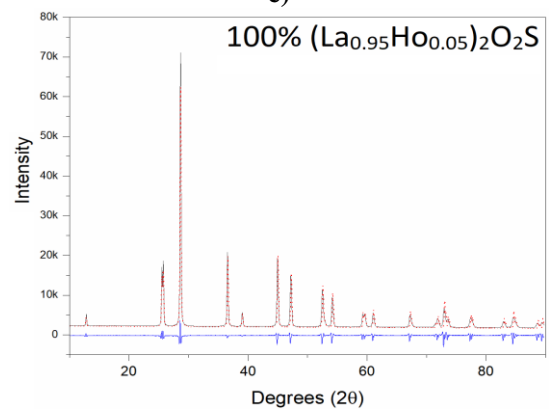
**d)**



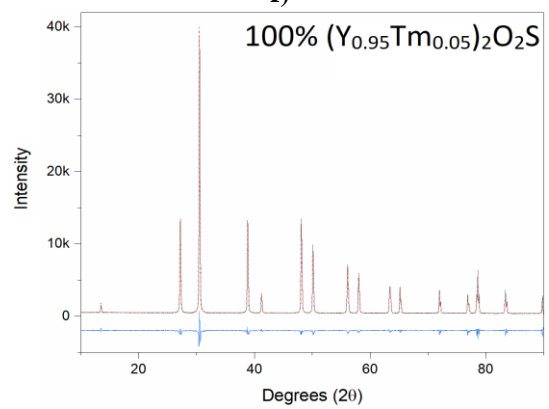
**e)**



**f)**



**g)**



**h)**

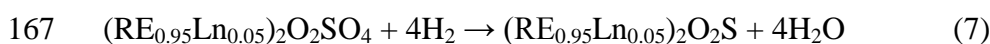
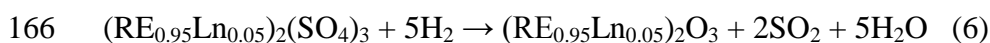
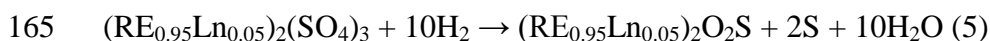
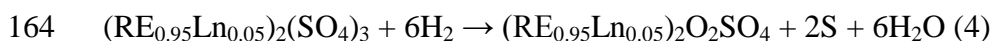
152

153 Fig.1. Difference Rietveld plot of: a,b)  $(RE_{0.95}Ln_{0.05})_2(SO_4)_3$ ; c,d)  $(RE_{0.95}Ln_{0.05})_2(SO_4)_3$ -  
 154  $(RE_{0.95}Ln_{0.05})_2O_2SO_4$ - $(RE_{0.95}Ln_{0.05})_2O_2S$  -  $(RE_{0.95}Ln_{0.05})_2O_3$ ; e,f)  $(RE_{0.95}Ln_{0.05})_2O_2S$  -  
 155  $(RE_{0.95}Ln_{0.05})_2O_3$ ; g,h)  $(RE_{0.95}Ln_{0.05})_2O_2S$

156 The same can be said about Figure 1, d; here, a similar phase composition is also observed,  
157 which is formed when the sample  $Y_2(SO_4)_3: Tm^{3+}$  (5 mol %) is processed in a hydrogen stream for  
158 1 hour at 620 °C.

159 With an increase in the treatment time in the hydrogen stream to 4 hours, at 620 °C, two  
160 phases were detected in the sample:  $(La_{0.95}Ho_{0.05})_2O_2S$  and  $(La_{0.95}Ho_{0.05})_2O_3$  (Fig. 1, e), as well as  
161  $(Y_{0.95}Tm_{0.05})_2O_2S$  and  $(Tm_{0.95}Ho_{0.05})_2O_3$  in Figure 1, f.

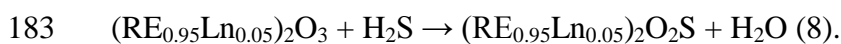
162 The following chemical equations correspond to the formation of the corresponding  
163 reduction products:



168 After 4 hours of carrying out the process at this temperature, according to x-ray phase  
169 analysis, the polycrystalline products consist of two phases:  $(RE_{0.95}Ln_{0.05})_2O_2S$ ,  $(RE_{0.95}Ln_{0.05})_2O_3$   
170 (Fig. 1, e, 1, f). In the products of intermediate transformations there are no compounds containing  
171  $SO_4^{2-}$  ions, which indicates the complete occurrence of the redox reaction. It should be noted that  
172 the content of the by-product, which is oxide, in the case of the reduction of yttrium sulfates is  
173 much higher (40.91 mol. %) than the corresponding compounds with lanthanum (23.13 mol.%).  
174 The thermodynamic stability of  $La_2O_2S$  is higher than that of  $Y_2O_2S$ , and that of  $Y_2O_3$  is higher  
175 than that of  $La_2O_3$  [26]. This may be another reason for the benefits of reaction 6.

176 Thus, during the reduction of rare earth sulfates in a hydrogen atmosphere for 4 hours, two-  
177 phase polycrystalline intermediate products are formed with a predominant content of the  
178 oxysulfide phase, which greatly facilitated the further sulfidation procedure.

179 A further, final step in the synthesis is the sulfidation reaction in an  $H_2S$  atmosphere. After  
180 processing the mixture of oxysulfide and oxide in a stream of hydrogen sulfide at 1000 °C for 4  
181 hours, according to the X-ray phase analysis, a single-phase sample of a solid solution of oxysulfide  
182 with the general formula  $(RE_{0.95}Ln_{0.05})_2O_2S$  is fixed (Figure 1, g, h):

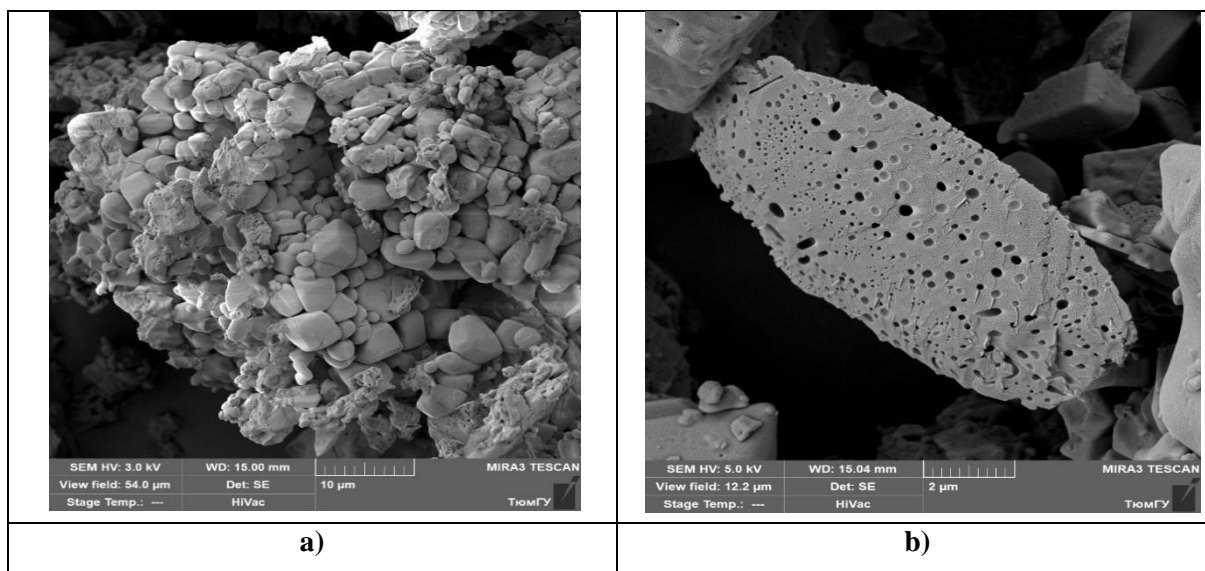


184 The particles of sulfate  $(Y_{0.95}Tm_{0.05})_2(SO_4)_3$  studied using a scanning electron microscope  
185 represent various formations: both oval and oblong, generally irregular in shape (Fig. 2, a) with  
186 sizes from 0.2 to 6 microns. Reason differences in the shape and size of the obtained particles and  
187 their adhesion to agglomerates is probably the uneven mixing during coprecipitation and co-  
188 crystallization. The particles of oxysulfide  $(La_{0.95}Tm_{0.01})_2O_2S$  obtained in the process of redox  
189 reactions are relatively large, oblong in shape, with sizes of  $5 \times 11 \mu m$ . The particle shown in  
190 Figure 2, b is flat, as if sanded, with small round holes  $d = 0.14-0.51 \mu m$  over its entire surface. The

191 morphological transformation is obviously due to elevated temperatures and the diffusion nature of  
 192 the reduction and sulfidation processes.

193 The sulfate  $(\text{La}_{0.95}\text{Tm}_{0.05})_2(\text{SO}_4)_3$  particles studied using a scanning electron microscope are  
 194 oblong-shaped formations (Fig. 2, a) with sizes from 2.5–3  $\mu\text{m}$ . The oxysulfide  $(\text{La}_{0.95}\text{Tm}_{0.01})_2\text{O}_2\text{S}$   
 195 particles obtained in the process of redox reactions are represented by agglomerates of 10–15  $\mu\text{m}$   
 196 (Fig. 2, b). The morphological transformation is obviously due to elevated temperatures and the  
 197 diffusion nature of the reduction and sulfidation processes.

198



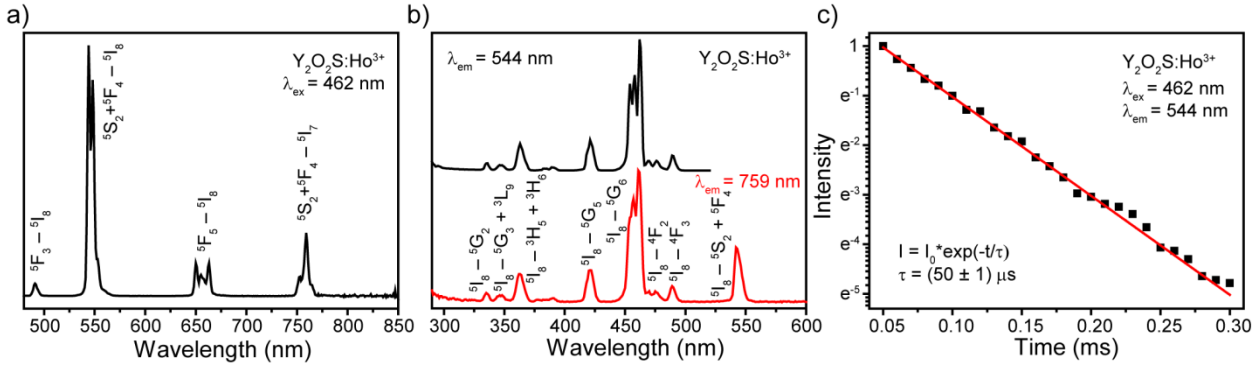
199 Fig. 2. SEM images of a)  $(\text{La}_{0.95}\text{Tm}_{0.01})_2(\text{SO}_4)_3$ ; b)  $(\text{La}_{0.99}\text{Tm}_{0.01})_2\text{O}_2\text{S}$

200 The excitation and emission spectra of  $\text{Y}_2\text{O}_2\text{S}:\text{Ho}^{3+}$  phosphor are presented in Fig. 3, a, 3, b.  
 201 Emission spectrum of  $\text{Y}_2\text{O}_2\text{S}:\text{Ho}^{3+}$  powder obtained upon 462 nm excitation consists of typical  
 202 narrow lines which can be assigned to following 4f-4f transitions:  $^5\text{F}_3-^5\text{I}_8$  (491 nm),  $^5\text{S}_2+^5\text{F}_4-^5\text{I}_8$   
 203 (544 and 548 nm),  $^5\text{F}_5-^5\text{I}_8$  (650, 655 and 663 nm) and  $^5\text{S}_2+^5\text{F}_4-^5\text{I}_7$  (753 and 759 nm) [27, 28].  
 204 Majority of emission bands include several lines because of Stark splitting of energy levels.  
 205 Excitation spectra of  $\text{Y}_2\text{O}_2\text{S}:\text{Ho}^{3+}$  powder were measured for two transitions:  $^5\text{S}_2+^5\text{F}_4-^5\text{I}_8$  (544 nm)  
 206 and  $^5\text{S}_2+^5\text{F}_4-^5\text{I}_7$  (759 nm). Spectral line positions did not depend on monitoring wavelength. Better  
 207 resolution in the first case is explained by less spectral slit width. The observed excitation lines  
 208 corresponds to  $^5\text{I}_8-^5\text{G}_2$  (336 nm),  $^5\text{I}_8-^5\text{G}_3+^3\text{L}_9$  (347 nm),  $^5\text{I}_8-^3\text{H}_5+^3\text{H}_6$  (363 nm),  $^5\text{I}_8-^5\text{G}_4$  (383 and  
 209 390 nm),  $^5\text{I}_8-^5\text{G}_5$  (421 nm),  $^5\text{I}_8-^5\text{G}_6$  (454, 458 and 462 nm),  $^5\text{I}_8-^4\text{F}_2$  (470, 477 nm),  $^5\text{I}_8-^4\text{F}_3$  (490  
 210 nm),  $^5\text{I}_8-^5\text{S}_2+^5\text{F}_4$  (542 nm) [29, 30]. Fig. 3c displays luminescence decay curve of  $\text{Y}_2\text{O}_2\text{S}:\text{Ho}^{3+}$   
 211 sample measured at the most prominent transition ( $\lambda_{\text{ex}} = 462 \text{ nm}$ ,  $\lambda_{\text{em}} = 544 \text{ nm}$ ). It is clearly seen,  
 212 that the experimental data demonstrate single exponential behavior:

213 
$$I = A \cdot e^{-\frac{t}{\tau}} \quad (1)$$

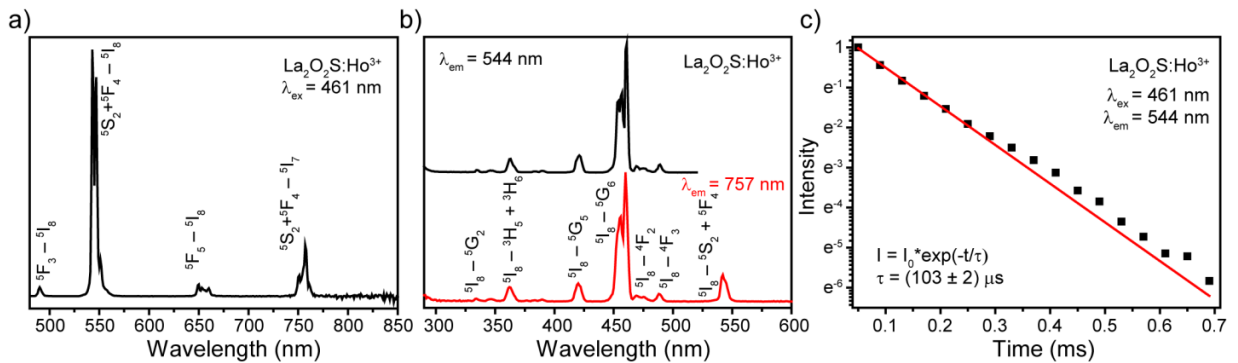


214 where  $\tau$  is observed lifetime. The observed lifetime of  $^5S_2+^5F_4$  excited level was found to be  
 215  $(50 \pm 1) \mu s$ .



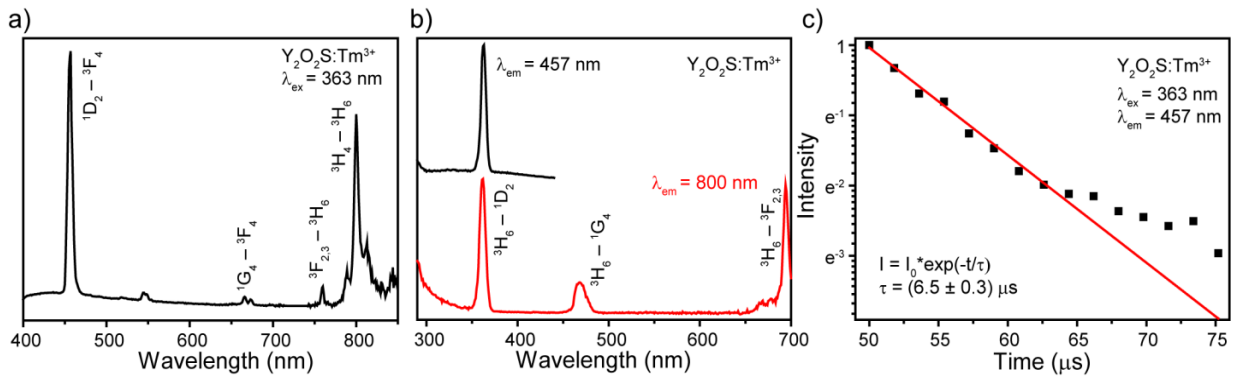
216  
 217 Fig. 3 a) Emission spectrum ( $\lambda_{ex} = 462$  nm), b) excitation spectra ( $\lambda_{em} = 544$  nm and 759 nm) and c)  
 218 luminescence decay of  $Y_2O_2S:Ho^{3+}$  powder.  
 219

220 To study host composition effect on photoluminescence properties, we regarded  
 221  $La_2O_2S:Ho^{3+}$  sample.  $Y_2O_2S$  and  $La_2O_2S$  have similar structure and symmetry, the only difference  
 222 is substitution of yttrium ( $r = 89$  pm) to lanthanum ( $r = 102$  pm) ions. Both hosts have the trigonal  
 223 space group  $D_{3d}^3$  and the point symmetry of the doping ion is  $C_{3v}$ . The crystal structure parameters  
 224 of studied oxysulfides differ in such a way that  $La_2O_2S$  has the larger interionic distances than  
 225  $Y_2O_2S$  one [21]. Emission spectrum of  $La_2O_2S:Ho^{3+}$  powder exhibited bands similar to those  
 226 observed in case of  $Y_2O_2S:Ho^{3+}$  sample:  $^5F_3-^5I_8$  (490 nm),  $^5S_2+^5F_4-^5I_8$  (544 and 547 nm),  $^5F_5-^5I_8$   
 227 (650, 653 and 660 nm) and  $^5S_2+^5F_4-^5I_7$  (751 and 757 nm) (Fig. 4, a). Small blue shift of lines and  
 228 redistribution between them were observed. The observed spectral shift can be explained as follows:  
 229 as the interionic distances increase, the energy levels of doping ions tend to approach the energy  
 230 levels of a free ion [21]. We monitored excitation spectra of  $La_2O_2S:Ho^{3+}$  phosphor for  $^5S_2+^5F_4-^5I_8$   
 231 (544 nm) and  $^5S_2+^5F_4-^5I_7$  (757 nm) transitions (Fig. 4, b). Both spectra are dominated by  $^5I_8-^5G_6$   
 232 transition (454, 457 and 461 nm). Almost all excitation bands also demonstrated aforementioned  
 233 blue shift. Luminescence kinetics of  $La_2O_2S:Ho^{3+}$  sample was measured at the most intensive line  
 234 centered at 544 nm upon 461 nm excitation (Fig. 4, c). Single exponential fitting of decay curve  
 235 allowed to obtain  $^5S_2+^5F_4$  lifetime for  $Ho^{3+}$ -doped  $La_2O_2S$  of  $(103 \pm 2) \mu s$ .



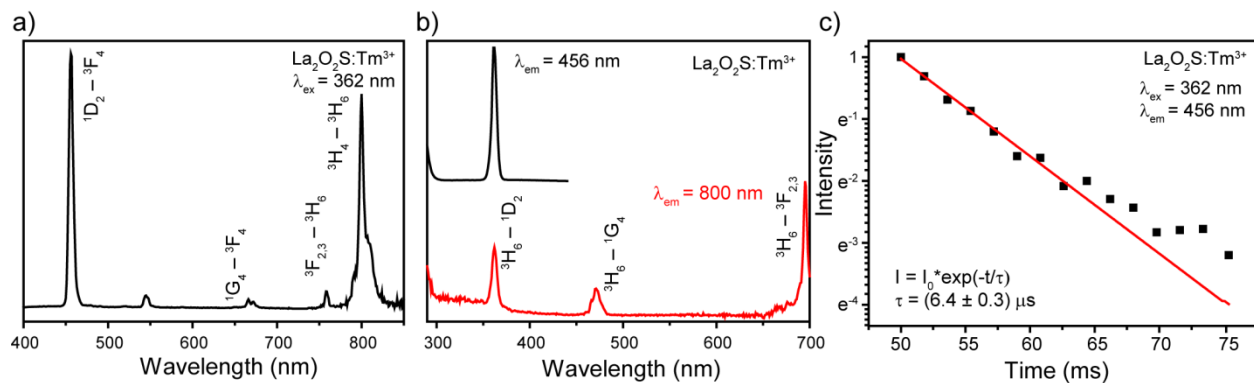
236  
 237 Fig. 4 a) Emission spectrum ( $\lambda_{ex} = 461$  nm), b) excitation spectra ( $\lambda_{em} = 544$  nm and 757 nm) and c)  
 238 luminescence decay of  $La_2O_2S:Ho^{3+}$  powder

239 Fig. 5, a shows emission spectrum of  $\text{Y}_2\text{O}_2\text{S}:\text{Tm}^{3+}$  sample upon 363 nm excitation measured  
 240 within spectral range of 400–850 nm. It displays narrow bands assigned to the 4f-4f transitions,  
 241 which are centered at 457 nm ( $^1\text{D}_2-^3\text{F}_4$ ), 666 and 673 nm ( $^1\text{G}_4-^3\text{F}_4$ ), 760 nm ( $^3\text{F}_{2,3}-^3\text{H}_6$ ) and 789,  
 242 800, 813 nm ( $^3\text{H}_4-^3\text{H}_6$ ) [31, 32]. Low-intensity bands near 550 nm are most probably attributed to  
 243 the emission of  $\text{Er}^{3+}$  impurity ions situated in the sample. As luminescence of  $\text{Tm}^{3+}$  ions in  $\text{Y}_2\text{O}_2\text{S}$  is  
 244 quite weak, we have also observed broad host emission situated in the 400–550 nm spectral region.  
 245 Excitation spectra of  $\text{Y}_2\text{O}_2\text{S}:\text{Tm}^{3+}$  phosphor were monitored at two transitions:  $^1\text{D}_2-^3\text{F}_4$  (457 nm)  
 246 and  $^3\text{H}_4-^3\text{H}_6$  (800 nm). Contrary to  $\text{Ho}^{3+}$ -doped samples, we measured excitation spectra for  
 247 transitions originated from different excited levels:  $^1\text{D}_2$  and  $^3\text{H}_4$ , respectively. These spectra consist  
 248 of sharp lines corresponding to intra-configurational f-f transitions:  $^3\text{H}_6-^1\text{D}_2$  (363 nm),  $^3\text{H}_6-^1\text{G}_4$   
 249 (468 nm) and  $^3\text{H}_6-^3\text{F}_{2,3}$  (694 nm) [31-32]. Noteworthy,  $^3\text{H}_6-^1\text{D}_2$  transition presented on both spectra  
 250 had the same spectral position. We monitored luminescence decay curve of  $\text{Y}_2\text{O}_2\text{S}:\text{Tm}^{3+}$  powder for  
 251 the most intense transition –  $^1\text{D}_2-^3\text{F}_4$ . Experimental data were fitted with single exponential decay  
 252 with sufficient accuracy (Adj.  $R^2 = 0.984$ ). The observed  $^1\text{D}_2$  lifetime was determined to be  
 253  $(6.5 \pm 0.3) \mu\text{s}$ .



254  
 255 Fig. 5 a) Emission spectrum ( $\lambda_{\text{ex}} = 363 \text{ nm}$ ), b) excitation spectra ( $\lambda_{\text{em}} = 457 \text{ nm}$  and  $800 \text{ nm}$ ) and c)  
 256 luminescence decay of  $\text{Y}_2\text{O}_2\text{S}:\text{Tm}^{3+}$  powder  
 257

258 The steady state luminescence spectra and luminescence kinetics of  $\text{La}_2\text{O}_2\text{S}:\text{Tm}^{3+}$  phosphor  
 259 are presented in Fig. 6. Host change led to the insignificant blue shift of spectral lines and intensity  
 260 redistribution. Emission spectrum includes  $^1\text{D}_2-^3\text{F}_4$  (456 nm),  $^1\text{G}_4-^3\text{F}_4$  (666 and 672 nm),  $^3\text{F}_{2,3}-^3\text{H}_6$   
 261 (758 nm) and  $^3\text{H}_4-^3\text{H}_6$  (800 nm) transitions. Excitation spectrum consists of  $^3\text{H}_6-^1\text{D}_2$  (362 nm),  
 262  $^3\text{H}_6-^1\text{G}_4$  (471 nm) and  $^3\text{H}_6-^3\text{F}_{2,3}$  (695 nm) transitions. Luminescence decay curve of  $^1\text{D}_2-^3\text{F}_4$   
 263 transition presented single exponential behavior, and  $^1\text{D}_2$  lifetime was found to be  $(6.4 \pm 0.3) \mu\text{s}$ .  
 264



265

266 Fig. 6 a) Emission spectrum ( $\lambda_{\text{ex}} = 362$  nm), b) excitation spectra ( $\lambda_{\text{em}} = 456$  nm and 800 nm) and c)  
 267 luminescence decay of  $\text{La}_2\text{O}_2\text{S}:\text{Tm}^{3+}$  powder.  
 268

269 An important parameter of phosphor is quantum yield ( $\phi$ ), which shows conversion  
 270 efficiency of absorbed photons into emitted ones. We measured quantum yield of synthesized  
 271 powders via absolute technique using integrating sphere. The obtained  $\phi$  values as well as  
 272 previously obtained photoluminescence characteristics are summarized in Table 1. The best  
 273 quantum yield of about 12% was found for  $\text{La}_2\text{O}_2\text{S}:\text{Ho}^{3+}$  sample. Analyzing obtained experimental  
 274 results, we can conclude that  $\text{La}_2\text{O}_2\text{S}$  is better host for holmium and thulium doping compared with  
 275  $\text{Y}_2\text{O}_2\text{S}$ . The same situation was observed for other lanthanides in these oxysulfide hosts [21].  
 276

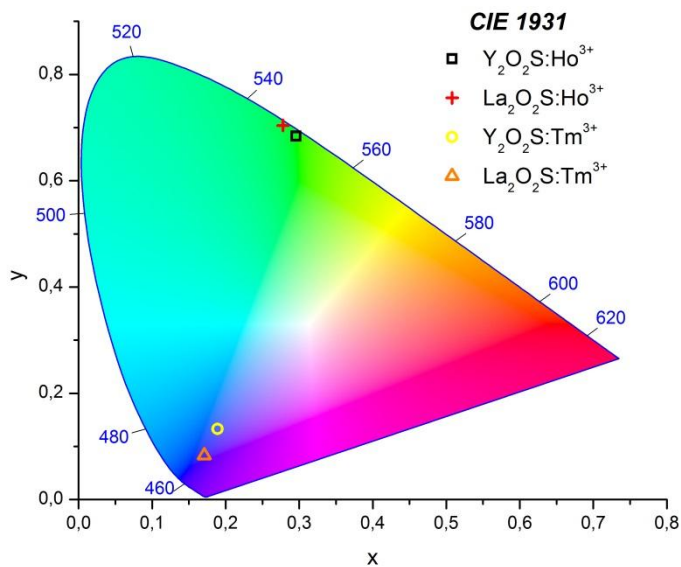
276

Material	$\lambda_{\text{em}}$ , nm	$\tau$ , $\mu\text{s}$	$\phi$ , %	CIE1931 chromaticity coordinates
$\text{Y}_2\text{O}_2\text{S}:\text{Ho}^{3+}$	491, 541, 663, 759	$50 \pm 1$	2.7	(0.296, 0.684)
$\text{La}_2\text{O}_2\text{S}:\text{Ho}^{3+}$	490, 544, 650, 757	$103 \pm 2$	12.3	(0.278, 0.704)
$\text{Y}_2\text{O}_2\text{S}:\text{Tm}^{3+}$	457, 544, 666, 760, 800	$6.5 \pm 0.3$	0.1	(0.189, 0.133)
$\text{La}_2\text{O}_2\text{S}:\text{Tm}^{3+}$	456, 545, 666, 758, 800	$6.4 \pm 0.3$	0.3	(0.171, 0.083)

277

278 Table 1. Main emission lines ( $\lambda_{\text{em}}$ ), lifetime ( $\tau$ ), quantum yield ( $\phi$ ) and CIE1931 chromaticity  
 279 coordinates of  $\text{RE}_2\text{O}_2\text{S}:\text{Ln}^{3+}$  samples.  
 280

281 Possible application of synthesized powders as a phosphor was studied via photometric  
 282 characterization. The Commission Internationale de L'Eclairage (CIE) chromaticity coordinates  
 283 calculated from measured emission spectra are listed in Table 1 and presented in Fig. 7. Despite  
 284 small spectral shift of emission lines in  $\text{Y}_2\text{O}_2\text{S}$  and  $\text{La}_2\text{O}_2\text{S}$  doped samples, chromaticity coordinates  
 285 vary significantly. Such behavior is elucidated by considerable intensity redistribution between  
 286 emission lines. Noteworthy, chromaticity coordinates of  $\text{Ho}^{3+}$  and  $\text{Tm}^{3+}$ -doped  $\text{La}_2\text{O}_2\text{S}$  samples are  
 287 close to green (0.300, 0.600) and blue (0.150, 0.060) colors – most commonly used primary colors  
 288 for display monitors and TV's (ITU-R BT.709 standard primaries). It makes synthesized powders  
 289 suitable for efficient green and blue phosphors application.



290  
291 Fig. 7. CIE1931 chromaticity coordinates of synthesized samples.  
292

#### 293 4. Conclusion

294 The sequence of phase formation of sulfates doped with rare earth elements ((La<sub>0.95</sub>Ln<sub>0.05</sub>)<sub>2</sub>(SO<sub>4</sub>)<sub>3</sub>  
295 and (Y<sub>0.95</sub>Ln<sub>0.05</sub>)<sub>2</sub>(SO<sub>4</sub>)<sub>3</sub> (Ln = Ho<sup>3+</sup>, Tm<sup>3+</sup>)) was studied during their sequential processing in a  
296 stream of H<sub>2</sub>, H<sub>2</sub>S. The phase and morphological certification of the obtained solid solutions of rare  
297 earth oxysulfides were carried out. Excitation and emission spectra of La<sub>2</sub>O<sub>2</sub>S:Ln<sup>3+</sup> и Y<sub>2</sub>O<sub>2</sub>S:Ln<sup>3+</sup>  
298 (Ln<sup>3+</sup>= Ho, Tm) included characteristic narrow bands corresponding to the 4f-4f intra-  
299 configurational transitions. Change of Y<sub>2</sub>O<sub>2</sub>S host to La<sub>2</sub>O<sub>2</sub>S resulted in small blue shift of emission  
300 lines which is caused by the larger interionic distances in the latter case. Study of luminescence  
301 decay showed that Ho<sup>3+</sup>-doped La<sub>2</sub>O<sub>2</sub>S powder had twice bigger lifetime compared with Ho<sup>3+</sup>-  
302 doped Y<sub>2</sub>O<sub>2</sub>S one, whereas Tm<sup>3+</sup>-doped samples have similar lifetime independently on host. The  
303 best quantum yield of about 12% was found for La<sub>2</sub>O<sub>2</sub>S:Ho<sup>3+</sup> sample. Chromaticity coordinates of  
304 Ho<sup>3+</sup> and Tm<sup>3+</sup>-doped La<sub>2</sub>O<sub>2</sub>S powders were close to green and blue standard colors, which makes  
305 them perspective for phosphor applications.

#### 306 Acknowledgments

307 Photoluminescence measurements were performed in “Center for Optical and Laser materials  
308 research” (St. Petersburg State University).

309

310

311

#### References

- 312 1. E.I. Sal'nikova, Yu.G. Denisenko, A.S. Aleksandrovsky, I.E. Kolesnikov, Lähderanta E.,  
313 P.O. Andreev, N.O. Azarapin, O.V. Andreev, S.A. Basova, A.V. Matigorov, Synthesis and Optical  
314 Properties RE<sub>2</sub>O<sub>2</sub>S:Ln (RE = La, Y; Ln = Ce, Eu, Dy, Er), J. Solid State Chem. 279 (2019) №  
315 120964. 1-6. <https://doi.org/10.1016/j.jssc.2019.120964>.  
316  
317 2. Yu.G. Denisenko, E.I. Sal'nikova, S.A. Basova, M.S. Molokeyev, A.S. Krylov, A.S.  
318 Aleksandrovsky, A.S. Orechenkov, V.V. Atuchin, S.S. Volkova, N.A. Khritokhin, O.V. Andreev,

- 319 Synthesis of Samarium Oxysulfate  $\text{Sm}_2\text{O}_2\text{SO}_4$  in the High-Temperature Oxidation Reaction and Its  
320 Structural, Thermal and Luminescent Properties, *Molecules*. 25 (2020) № 1330. 1-15.  
321 <https://doi.org/10.3390/molecules25061330>.  
322
- 323 3. Yu.G. Denisenko, M.S. Molokeyev, A.S. Krylov, A.S. Alecsandrovsky, A.S. Oreshonkov, V.V.  
324 Atuchin, N.O. Azarapin, P.E. Plyusnin, E.I. Sal'nikova, O.V. Andreev, High-temperature oxidation  
325 of europium (II) sulfide, *J. Ind. Eng. Chem.* 79 (2019) 62-70.  
326 <https://doi.org/10.1016/j.jiec.2019.05.006>.  
327
- 328 4. P.O. Andreev, E.I. Sal'nikova, O.V. Andreev, Yu.G. Denisenko, I.M. Kovenskii, Synthesis and  
329 Upconversion Luminescence Spectra of  $(\text{Y}_{1-x-y}\text{Yb}_x\text{Er}_y)_2\text{O}_2\text{S}$ , *Inorg. Mater.* 53 (2) (2017) 200-206.  
330 <https://doi.org/10.1134/S0020168517020029>.  
331
- 332 5. S. W. Kim, T. Hasegawa, T. Abe, H. Nakagawa, S. Hasegawa, K. Seki, K. Toda, K. Uematsu, T.  
333 Ishigaki, M. Sato. Abnormal improvement in emission of lanthanum oxysulfide phosphor  
334  $\text{La}_2\text{O}_2\text{S}:\text{Tb}^{3+}$  synthesized by a novel method, thermal decomposition in eutectic molten salt //  
335 *Ceramic International*. 42 (2016) 10389-10392. <https://doi.org/10.1016/j.ceramint.2016.03.176>.  
336
- 337 6. Y. Yang, C. Mi, F. Yu, C. Guo, G. Li, J. Zhang, L. Liu, Y. Liu, X. Li, Optical thermometry based  
338 on the upconversion fluorescence from  $\text{Yb}^{3+}/\text{Er}^{3+}$  codoped  $\text{La}_2\text{O}_2\text{S}$  phosphor // *Ceramics*  
339 *International*. 40 (2014) (7) 9875-9880. <https://doi.org/10.1016/j.ceramint.2014.02.081>.  
340
- 341 7. I.A. Razumkova, Synthesis of  $\text{NaYF}_4$  compounds from sulfide precursors, *J. Fluorine Chem.* 205  
342 (2018) 1-4. <https://doi.org/10.1016/j.jfluchem.2017.10.012>.  
343
- 344 8. I.A. Razumkova, Y.G. Denisenko, A.N. Boyko, D.A. Ikonnikov, A.S. Aleksandrovsky, N.O.  
345 Azarapin, O.V. Andreev, Synthesis and upconversion luminescence in  $\text{LaF}_3:\text{Yb}^{3+}, \text{Ho}^{3+}$ ,  
346  $\text{GdF}_3:\text{Yb}^{3+}, \text{Tm}^{3+}$  and  $\text{YF}_3:\text{Yb}^{3+}, \text{Er}^{3+}$  obtained from sulfide precursors, *Z. Anorg. Allg. Chem.* 645  
347 (2019) 1393-1401. <https://doi.org/10.1002/zaac.201900204>.
- 348 9. I.E. Kolesnikov, E.V. Golyeva, E. Lähderanta, A.V. Kurochkin, M.D. Mikhailov, Ratiometric  
349 thermal sensing based on  $\text{Eu}^{3+}$ -doped  $\text{YVO}_4$  nanoparticles, *J. Nanopart. Res.* 18 (12) (2016) 354.  
350 <https://doi.org/10.1007/s11051-016-3675-8>.
- 351 10. I.E. Kolesnikov, A.A. Kalinichev, M.A. Kurochkin, D.V. Mamonova, E.Yu. Kolesnikov, A.V.  
352 Kurochkin, E. Lähderanta, M.D. Mikhailov,  $\text{Y}_2\text{O}_3:\text{Nd}^{3+}$  nanocrystals as ratiometric luminescence  
353 thermal sensors operating in the optical windows of biological tissues, *J. Lum.* 204 (2018) 506–512.  
354 <https://doi.org/10.1016/j.jlumin.2018.08.050>.  
355
- 356 11. G. Jiang, X. Wei, Y. Chen, C. Duan, M. Yin, B. Yang, W. Cao, Luminescent  $\text{La}_2\text{O}_2\text{S}:\text{Eu}^{3+}$   
357 nanoparticles as non-contact optical temperature sensor in physiological temperature range,  
358 *Materials Letters*. 143 (2015) 98-100. <https://doi.org/10.1016/j.matlet.2014.12.057>.  
359
- 360 12. M. Aryal, S.W. Allison, K. Olenick, F. Sabri, Flexible thin film ceramics for high temperature  
361 thermal sensing applications, *Optical Materials*. 100 (2020) № 109656 (1-11).  
362 <https://doi.org/10.1016/j.optmat.2020.109656>.  
363
- 364 13. S. Tan, D. Li. Enhancing Oxygen Storage Capability and Catalytic Activity of Lanthanum  
365 Oxysulfide ( $\text{La}_2\text{O}_2\text{S}$ ) Nanocatalysts by Sodium-and Iron/Sodium-Doping // *ChemCatChem*. 10  
366 (2018) 550–558. <https://doi.org/10.1002/cctc.201701117>.  
367

- 368 14. W. Zhang, I. W. C. E. Arends, K. Djanashvili, Nanoparticles of oxysulfate/oxysulfide for  
369 improved oxygen storage/release, Dalton Transactions. 45 (2016) 14019-14022.  
370 <https://doi.org/10.1039/C6DT01667G>.  
371
- 372 15. T.W. Chou, S. Mylswamy, R.S. Liu, S.Z. Chuang, Eu substitution and particle size control of  
373  $Y_2O_2S$  for the excitation by UV light emitting diodes, Solid State Communications. 136 (2005)  
374 205–209. <https://doi.org/10.1016/j.ssc.2005.07.032>.  
375
- 376 16. P. Han, Y. Zhu, J. Li, T. Li, X. Jiang, C. Zhang, B. Jiao, Q. Wu, Upconversion White Light  
377 Output in  $(Y_{0.9}Gd_{0.1})_2O_2S$  Matrix Tri-Doped with  $Yb^{3+}/Tm^{3+}/Er^{3+}$  or  $Yb^{3+}/Tm^{3+}/Ho^{3+}$ , Nanoscience  
378 and Nanotechnology Letters. 9 (4) (2017) 586–591. <https://doi.org/10.1166/nnl.2017.2361>.  
379
- 380 17. G. Ajithkumar, B. Yoo, D.E. Goral, P.J. Hornsby, A.L. Lin, U. Ladiwala, V.P. Dravide, D.K.  
381 Sardara, Multimodal bioimaging using a rare earth doped  $Gd_2O_2S:Yb/Er$  phosphor with  
382 upconversion luminescence and magnetic resonance properties, J. Mater. Chem. B. 1 (2013) 1561-  
383 1572. <https://doi.org/10.1039/c3tb00551h>.  
384
- 385 18. Q. Ju, D. Tu, Y. Liu, H. Zhu, X. Chen, Lanthanide-Doped Inorganic Nanocrystals as  
386 Luminescent Biolabels, Combinatorial Chemistry & High Throughput Screening. 15 (7) (2012) 580  
387 -594. <https://doi.org/10.2174/138620712801619177>.  
388
- 389 19. X. Wang, Z. Hu, Q. Zhu, J. Li, X. Sun,  $La_2O_2SO_4:RE/Yb$  new phosphors for near infrared to  
390 visible and near infrared upconversion luminescence (RE=Ho, Er, Tm), Journal of the American  
391 Ceramic Society. 101 (7) (2018) 2701–2706. <https://doi.org/10.1111/jace.15477>.  
392
- 393 20. S.A. Osseni, S. Lechevallier, M. Verelst, P. Perriat, J. Dexpert-Ghys, D. Neumeyer, R. Garcia, F.  
394 Mayer, K. Djanashvili, J.A. Peters, E. Magdeleine, H. Gros-Dagnac, P. Celsis, R. Mauricot, Gadolinium  
395 oxysulfide nanoparticles as multimodal imaging agents for  $T_2$ -weighted MR, X-ray tomography and  
396 photoluminescence, Nanoscale. 6 (2014) 555-564. <https://doi.org/10.1039/C3NR03982J>.  
397
- 398 21. H. Ratinen, X-Ray-Excited Optical Fluorescence of Ten Rare Earth Ions in  $Y_2O_2S$ ,  $La_2O_2S$ , and  
399  $Gd_2O_2S$ , Phys. Stat. Sol. 12 (1972) 447-451. <https://doi.org/10.1002/pssa.2210120211>.  
400
- 401 22. Manashirov O.Ya., Georgobiani A.N., Gutan V.B., et al. Synthesis and IR-Excited  
402 Luminescence of  $(Y_{1-x}Tm_x)_2O_2S$  Solid Solutions // Inorganic Materials. 49 (3) (2013) 278 - 282.  
403 <https://doi.org/10.1134/S0020168513020131>.  
404
- 405 23. K.C. Bleijenberg K. C., F.A. Kellendonk, Two-photon excited luminescence of  
406 thulium-activated lanthanum oxysulfide ( $La_2O_2S-Tm^{3+}$ ), J. Chem. Phys. 73 (1980). 3586.  
407 <https://doi.org/10.1063/1.440583>.  
408
- 409 24. A.O. Semiyov, Yu.G. Denisenko, J.K. Fatombi, E.I. Sal'nikova, O.V. Andreev, Synthesis and  
410 characterization of  $Ln_2O_2SO_4$  (Ln = Gd, Ho, Dy and Lu) nanoparticles obtained by coprecipitation  
411 method and study of their reduction reaction under  $H_2$  flow, J. Nanostuct. Chem. 7 (2017) 337-343.  
412 <https://doi.org/10.1007/s40097-017-0243-4>.  
413
- 414 25. Bruker AXS TOPAS V4: General profile and structure analysis software for powder diffraction  
415 data. User's Manual. Bruker AXS, Karlsruhe, Germany. 2008.  
416
- 417 26. Suponitskiy, Y.L. Thermal Chemistry of Oxygen-Containing Compounds of REE Elements and  
418 Elements of Group VI. Thesis of Doctor of Science in Chemistry, D. Mendeleev University of  
419 Chemical Technology of Russia, Moscow, Russia, 2002.  
420

- 421 27. L. Guo, Yu. Wang, J. Zhang, Y. Wang, P. Dong. Near-infrared quantum cutting in Ho<sup>3+</sup>, Yb<sup>3+</sup>-  
422 codoped BaGdF<sub>5</sub> nanoparticles via first-and second-order energy transfers, *Nanoscale Res Lett.* 7.  
423 636 (1) (2012) 1-7. <https://doi.org/10.1186/1556-276X-7-636>.  
424
- 425 28. B. Suresh, Ya. Zhydachevskii, M.G. Brik, A. Suchocki, M. Srinivasa Reddy, M. Piasecki, N.  
426 Veeraiah, Amplification of green emission of Ho<sup>3+</sup> ions in lead silicate glasses by sensitizing with  
427 Bi<sup>3+</sup> ions, *Journal of Alloys and Compounds.* 683 (2016) 114-122. DOI:  
428 10.1016/j.jallcom.2016.05.056.  
429
- 430 29. N.S. Hussain, N. Ali, A.G. Dias, M.A. Lopes, J.D. Santos, S. Buddhudu, Absorption and  
431 emission properties of Ho<sup>3+</sup> doped lead–zinc–borate glasses, *Thin Solid Films.* 515 (1) (2006) 318 –  
432 325. <https://doi.org/10.1016/j.tsf.2005.12.085>.  
433
- 434 30. C.R. Kesavulu, H.J. Kim, S.W. Lee, J. Kaewkhao, N.Wantana, S. Kothan, S. Kaewjaeng,  
435 Optical spectroscopy and emission properties of Ho<sup>3+</sup>-doped gadolinium calcium silicoborate  
436 glasses for visible luminescent device applications, *Journal of Non-Crystalline Solids.* 474 (2017)  
437 50-57. <https://doi.org/10.1016/j.jnoncrysol.2017.08.018>.  
438
- 439 31. O.A. Lopez, J. McKittrick, L.E. Shea, Fluorescence properties of polycrystalline Tm<sup>3+</sup> -  
440 activated Y<sub>3</sub>Al<sub>5</sub>O<sub>12</sub> in the visible and near IR ranges, *Journal of Luminescence.* 71 (1997) 1-11.  
441 [https://doi.org/10.1016/S0022-2313\(96\)00123-8](https://doi.org/10.1016/S0022-2313(96)00123-8).  
442
- 443 32. J.X. Lefu, M.J. Deng, H. Liu, B. Ma, M. Guan, L. Liao, G. Lv, Up-conversion luminescence  
444 properties and energy transfer of Tm<sup>3+</sup>/Yb<sup>3+</sup> co-doped BaLa<sub>2</sub>ZnO<sub>5</sub>, *Journal of Solid State*  
445 *Chemistry.* 231 (2015) 212-216. <https://doi.org/10.1016/j.jssc.2015.07.046>Get rights and content.  
446
- 447 33. I.E. Kolesnikov, M.A. Kurochkin, A.A. Kalinichev, E.Yu. Kolesnikov, E. Lähderanta, Optical  
448 temperature sensing in Tm<sup>3+</sup>/Yb<sup>3+</sup>-doped GeO<sub>2</sub>-PbO-PbF<sub>2</sub> glass ceramics based on ratiometric and  
449 spectral line position approaches, *Sensors and Actuators A: Physical.* 284 (2018) 251-259.  
450 <https://doi.org/10.1016/j.sna.2018.10.039>.